**Cell Reports**

**Supplemental Information**

# Mammalian Reverse Genetics without Crossing Reveals *Nr3a* as a Short-Sleeper Gene

**Genshiro A. Sunagawa, Kenta Sumiyama, Maki Ukai-Tadenuma, Dimitri Perrin, Hiroshi Fujishima, Hideki Ukai, Osamu Nishimura, Shoi Shi, Rei-ichiro Ohno, Ryohei Narumi, Yoshihiro Shimizu, Daisuke Tone, Koji L. Ode, Shigehiro Kuraku, and Hiroki R. Ueda**

# SUPPLEMENTAL EXPERIMENTAL PROCEDURES

### A Computational Model to Estimate the Minimum Efficiency to Generate Whole-body KO Mice by Multiple-target CRISPR Methods

A computational model estimated the efficiency of different CRISPR methods for generating whole-body knockout mice as follows. When sufficient Cas9 are provided, the efficiency of the single-gene mono-allelic knockout *P* can be described as:

$$P = \frac{S}{K+S}$$

, where total gRNA concentration and the dissociation constant between the gRNA and its target site are defined as *S* and *K*, respectively. This simple phenomenological model is adopted as the first-order approximation of the observed saturation in CRISPR-mediated DNA cutting. It describes the net effect, which is therefore intended to mechanistically include the known biochemical processes carried on during DNA cutting (e.g. PAM site binding, as well as, Cas9 remaining bonded to the cut DNA site on both strands following a cut).

When a single allele is targeted by three different gRNAs at the concentration *S/3* with dissociation constants ($K_1$, $K_2$, and $K_3$) between each gRNA and its target site, the single-gene mono-allelic KO efficiency *P* can be described as:

$$P = 1 - \left(\frac{K_1}{K_1+S/3}\right)\left(\frac{K_2}{K_2+S/3}\right)\left(\frac{K_3}{K_3+S/3}\right)$$

The concentration of each gRNA is *S/3* to keep total gRNA concentration as *S*.

Now, to include the recovery rate from single-site damage ($\alpha$) is introduced as the probability to recover of a single target site from a damaged state to an intact

state. When $\alpha$ is considered, the single-gene mono-allelic KO efficiency $P$ for a single-target method (**Figure 1B**) can be described as:

$$P = \frac{S(1-\alpha)}{K+S}$$

Similarly, the single-gene mono-allelic KO efficiency $P$ for a triple-target CRISPR method (**Figure 1B**) can be described as:

$$P = \frac{S(K_1K_2+K_2K_3+K_3K_1)(1-\alpha)+S^2(K_1+K_2+K_3)(1-\alpha^2)+S^3(1-\alpha^3)}{(K_1+S/3)(K_2+S/3)(K_3+S/3)}$$

When a single allele is targeted by $N$ different sites, the dissociation constant between each gRNA and its target site is defined as $K_i$ $(i=1\cdots N)$. The single-gene mono-allelic KO efficiency $P$ for a $N$-tuple-target method (**Figure S1A**) can be then described as:

$$P = \frac{S(K_1\cdots K_{N-1}+\cdots+K_2\cdots K_N)(1-\alpha)+\cdots+S^{N-1}(K_1+\cdots+K_N)(1-\alpha^{N-1})+S^N(1-\alpha^N)}{\prod_{i=1}^{N}(K_i+S)}$$

In our simulations, the single-gene mono-allelic KO efficiency $P$ was calculated 1,000 times for each given $\alpha$, $N$ and $S$. In every time of calculation, one set of $K$ (1, 3, and $N$ for single-, triple-, and $N$-tuple-target methods, respectively) were picked up randomly from a log-normal distribution whose geometric mean and geometric standard deviation as 1.0 and 2.5, respectively (**Figure S1B**). Without loss of generality, we can use 1.0 for the geometric mean of the distribution of the dissociation constant $K$. In order to estimate its geometric standard deviation, we first estimated three gRNA dissociation constants from the SSA assay for three gRNAs for *Tyr* gene ($K_1$ = 2.32203, $K_2$ = 1.16562 and $K_3$ = 0.369466 for Tyr-1, Tyr-2 and Tyr-3, respectively, **Figure 1D**). We note that $K$ is estimated as an inverse-proportional value to the DNA-cleavage efficiency measured from SSA assays. Since the geometric standard

deviation of these estimated *K* values was 2.53097, we used 2.5 for the geometric standard deviation. In order to estimate the efficiency of single-gene biallelic KO, double-gene biallelic KO, and triple-gene biallelic KO, we calculated $P^2$, $P^4$ *and* $P^6$, respectively when $\alpha$ = 0.10 (**Figure S1A**). Since there is uncertainty for $\alpha$ and *S in vivo*, we also calculated single-gene biallelic KO efficiency $P^2$ with different values of $\alpha$ and *S* (**Figure S1C**, $\alpha$ = 0.05, 0.10, 0.15, and *S* = 5, 10, 15, respectively). We note that calculated KO efficiencies for multiple-target methods (*N* > 1) predict the "minimum" efficiency of KO since we did not include, for its simplicity, the probability of other type of mutations in the multiple-target CRISPR models (e.g. large deletions induced by multiple-target CRISPR methods), which is difficult for a DNA repair system to recover back to the intact state.

To estimate the realistic values for $\alpha$ and *S*, we constructed three single-target CRISPR models with different dissociation constants ($K_1$ = 2.32203, $K_2$ = 1.16562 and $K_3$ = 0.369466) estimated from the SSA assay results for Tyr-1, Tyr-2, and Tyr-3, respectively. We compared that these models with the experimental results of single-target CRISPR (36.0%, 54.2% and 64.7% for Tyr-1, Tyr-2 and Tyr-3, respectively), and used a least squares method to estimate the realistic values for a recovery rate of mutation ($\alpha$ = 0.136428) and total gRNA concentration (*S* = 5.7248), respectively. We then performed 1,000 simulations to calculate single-gene biallelic KO efficiency ($P^2$) for single-target (*N* = 1) and triple-target (*N* = 3) CRISPR models with $\alpha$ = 0.136 and *K*, which are randomly picked up from the log-normal distribution in **Figure S1B**. As a results, single-gene biallelic KO efficiency ($P^2$) for single-target (*N* = 1) and triple-target (*N* = 3) CRISPR models at *S* = 5.7248 are 0.512 ± 0.138 and 0.826 ± 0.098 (mean ± SD), respectively (**Figure S1F**), indicating that a triple-target CRISPR method is much more efficient than a single-target CRISPR method when we used the realistic parameter values for $\alpha$ and *S*. In addition, the triple-target

strategy using the mixture of *Cas9* mRNA and three gRNAs achieved almost perfect efficiency (97.5%, **Figures 1E and 1F**), which is even more efficient than the predicted minimum efficiency (82.6%) (**Figure S1F**).

**Sleep Analysis by EEG/EMG**

We anesthetized the animals and implanted telemetry transmitters (F20-EET, DSI) into them for EEG/EMG recording. The detailed methods were described previously (Sunagawa et al., 2013). The recorded data were analyzed by the FASTER method followed by a 16-second-rule filter. This rule only allows sleep or wake epochs lasting longer than 16 seconds (two epochs in this study). If the automatically staged results include sleep or wake episodes sized less than 16 seconds, these epochs will be converted to the stage just before the episode started.

**Equivalent Electrical Circuit Simulation of the SSS System.**

Introducing the Laplace transform, the SSS system can be modeled as an electrical circuit (**Figure 3B**). Reducing the physical properties of the SSS components to those of electrical circuit elements, the pressure difference detected by the sensor can be predicted through simulation. Using these results, we optimized two variable components in the SSS system, i.e., a resistance ($R_1$) and a capacitance ($C_2$).

The mathematical descriptions of the model are as follows. When the total air flow is $I$, the flow can be divided into $I_1$ and $I_2$, which are the flow to the chamber and the sensor (**Figure 3B**), respectively. How $I$ is divided into $I_1$ and $I_2$ is determined

by the ratio of conductance of the chamber and the sensor unit. This conductance can be described in the Laplace domain as:

$$G_1(s) = \frac{1}{C_1 s + \frac{1}{R_1}}$$

$$G_2(s) = R_2 + \frac{1}{C_2 s}$$

where $G_1$ and $G_2$ denote the conductance of the SSS chamber and the pressure sensor unit, respectively. $C_1$ is the capacitance of the SSS chamber, $R_1$ is the resistance of the SSS chamber, $R_2$ is the resistance of the pressure sensor, and $C_2$ is the capacitance of the sensor. Using $G_1$ and $G_2$, the air flow to the sensor can be described as:

$$I_2 = I - I_1 = \frac{G_1}{G_1 + G_2} I$$

This equation can be interpreted as $I_2$ is a value that $I$ is amplified by $G_1/(G_1+G_2)$. Now, $R_2$ is the resistance of the sensor and $C_1$ depends on the volume of the chamber. Using a simple flow meter and a flow pump and the pressure sensor, we estimated $R_2$ and $C_1$ as 152 Pa·s/ml and 0.018 ml/Pa, respectively. Because this whole circuit can be treated as a band-pass filter, our goal was to optimize $R_1$ and $C_2$ to maximize the gain of $G_1/(G_1+G_2)$ over the physiological respiration frequency of mice. We ran computer simulations and selected 172 Pa·s/ml and $6.12 \times 10^{-5}$ ml/Pa as an optimal value for $R_1$ and $C_2$ in our environment (**Figure 3C**).

**Fully-Automated Sleep/wake Phenotype Analysis by SSS Annotation Pipeline**

The SSS annotation pipeline realizes fully automated sleep/wake phenotype analysis from respiration data of mice. The basic staging strategy was based on the FASTER method, which automatically stages the sleep state from EEG/EMG recordings (Sunagawa et al., 2013) (**Figure S2B**).

The SSS annotation pipeline is composed of three major steps (character extraction, clustering, and annotation). In the character extraction step, the recorded respiratory flow data are split into 8-second-length segments (called “epochs”). Each epoch of respiratory-flow time-domain data are next converted by fast Fourier transform (FFT) into frequency-domain data, the respiration power spectra. We used the power up to the maximum frequency, called Nyquist frequency (i.e. half of the sampling frequency), which corresponds to 125 Hz in this study because the respiratory flow was recorded at 250 Hz. Characters of respiration power spectra are then extracted by principal component analysis (PCA). The top three principal components were used in the following analysis.

In the following clustering step, we used the nonparametric density estimation clustering method (Azzalini and Torelli, 2007) to cluster the epochs. This clustering method automatically selects the number of clusters, and therefore it is powerful to cluster certain datasets without a priori model or without information on the number of clusters. A 6-day length data includes 64800 epochs. Entire epochs are divided into 12 group. Each group including 5400 epochs is used for a single-run of clustering. There are two parameters used for this clustering. One is the smoothing factor $h_{mult}$ which is used when the probability density is estimated from the given data. The other is $N_{grid}$, which affects the grid density for scanning the cluster core from the estimated probability density. We used 0.80 and 270 as $h_{mult}$ and $N_{grid}$, respectively.

In the final annotation step, each cluster is annotated according to the statistical value of characteristics for each cluster. During sleep the respiratory pattern represents a slow and regular flow while during wake the flow become fast and highly fluctuated (**Figure S2A**). This time-domain observation in sleep turns out to have a peaky shape in power spectrum due to the regular respiration patterns. On the other hand, during waking, the power spectrum of the respiratory flow tends to include wide range of spectra, therefore showing relatively more uniform power spectrum due to its fast and fluctuated respiration patterns. Focusing on these characteristic patterns in the frequency domain, we classified “sleep” and “awake” states by using larger and smaller skewness of the epoch’s power, respectively. “Sleep” state exhibits larger skewness than awake state because of its higher power for a narrower range of frequency and lower power for other range of frequency, which will make the distribution of sleep-epoch’s power positively skewed. Therefore, we defined when the median of skewness of epoch’s power spectrum in one cluster is within the 49th percentile (from the lowest value) of skewness of power spectrum of entire epochs, the cluster is annotated as “awake,” otherwise as “sleep”. After each cluster is annotated by skewness of power spectrum, the two epoch rule (one state continues at least two epochs) is applied to the results and the staging completes. All steps were fully-automated and unsupervised, which allows a highly-objective and reproducible sleep/wake phenotype analysis. The source code of the SSS analysis is available at **Supplemental Code S1 (https://goo.gl/teteJM)**.

The SSS technology is applied only to mice in this study. However, it might be possible to extend this method to larger organisms such as primates and human. SSS only uses a simple pressure sensor to detect the respiration pattern. Therefore, the subject needs to be placed in a semi-closed area for monitoring. Applications could be sleep monitors for babies in the incubator, or in the car for drivers.

**Calculation of Sleep/wake Parameters**

Four sleep/wake parameters are mainly used in this study. One is the "sleep time." This is the length of time that an animal's status is staged as sleep over a given period of time. The second is the "amplitude of sleep," or simply the "amplitude." When an animal's sleep time is recorded for $D$ days and summed in the $B$-minutes-bin, the sleep time of the $k^{th}$ bin is expressed as $T_k$, where

$$1 < k < DL_B$$

and

$$L_B = \frac{1440}{B}$$

The average sleep time of the $m^{th}$ bin of the day is expressed as

$$\tilde{T}_m = \frac{1}{D}\sum_{i=1}^{D} T_{m+L_B(i-1)}$$

When the mean of all bins is expressed as

$$E_{\tilde{T}} = \frac{1}{L_B}\sum_{i=1}^{L_B} \tilde{T}_i$$

the amplitude $A$ is defined as

$$A = \frac{1}{E_{\tilde{T}} L_B}\sum_{i=1}^{L_B} (\tilde{T}_i - E_{\tilde{T}})^2$$

The amplitude value differs with the bin “size” (i.e., duration) used to integrate the sleep time. We used a 10-min bin size in this study for amplitude calculation. Circadian and/or daily rhythmicity is expressed as a larger sleep/wake amplitude value.

The third and fourth statistics are the transition probability between sleep and awake states. In this study, sleep staging is undergone every 8 seconds. This minimal unit of sleep/wake state is called a segment (or an epoch). When we focus on two consecutive epochs, there are four possible sets of state. They are sleep to awake, awake to sleep, two sleep repeats and two wake repeats. When $N_{mn}(X)$ is defined as a number of transitions from state m to n (m,n $\subseteq$ {sleep, awake}) within the period X,

$$P_{ws} = \frac{N_{ws}}{N_{ws}+N_{ww}},\ P_{sw} = \frac{N_{sw}}{N_{ss}+N_{sw}}\ .$$

The two transition probabilities, $P_{ws}$ and $P_{sw}$, which are independent of each other, are indirect stabilization parameters that negatively reflect the stabilization of the awake state ($P_{ww}$) and sleep state ($P_{ss}$), respectively ($P_{ws}$ = 1 - $P_{ww}$, and $P_{sw}$ = 1 - $P_{ss}$). We think $P_{WS}$ and $P_{SW}$ are useful to experimentally test the sleep models which try to provide sleep-wake temporal architecture (Diniz Behn and Booth, 2011) because the transition probabilities can be quantified by SSS.

**Pharmacological Administration**

Methamphetamine (Philopon, Sumitomo Dainippon Pharma, Lot #006281) was diluted with natural saline to be 3 mg/kg at 100 µl of solution. The vehicle was natural saline. Each mouse received an i.p. injection at ZT2.

Diazepam (Horizon, Maruishi Pharmaceutical, Lot #3Y140) was diluted with natural saline to be 5 mg/kg at 300 µl of solution. The vehicle was natural saline. Each mouse received an i.p. injection at ZT13 under dark conditions.

Every animal used for pharmacological experiment was C57BL/6N male mice (6 to 8-week-old). Mice were assigned arbitrarily to control or treatment groups except the animals used in dual recording for EEG/EMG and SSS. In the dual recording, the control animals used in DZP i.p. injection were used for MAP i.p. injection after 4 days of recovery period.

**Design of Target Sequences for gRNA**

The target sequences for *Tyr* (**Figure 1C**) were designed using Jack Lin's on-line CRISPR gRNA finder (http://spot.colorado.edu/~slin/cas9.html). The target sequences for *Bmal1*, *Cry1*, *Cry2*, *Per1*, *Per2, Hcrt* (**Figures S4A-C and S4K**), *Nr1*, *Nr2a*, *Nr2b*, *Nr2c*, *Nr2d*, *Nr3a* (set 1 and 2), and *Nr3b* (**Figures S5A-G and S6A**) were designed using the on-line CRISPR guide RNA Design tool (http://cas9.cbi.pku.edu.cn/index.jsp)(Ma et al., 2013). Possible off-target sequences within the mouse genome for each target sequence were checked using the CRISPR Design Tool (http://tools.genome-engineering.org) (Ran et al., 2013).

The alternative target sequences for *Tyr* (set 2 and 3, **Figure 7D**) were selected from the list resulting from the mm10 CRISPR/Cas9 database (**http://www.crispr.riken.jp/**).

**Construction of the pGL3-SSA Plasmid for the Single-strand Annealing (SSA) Assay**

Two partial fragments of the pGL3-control vector (Promega), containing the 5'- or 3'-partial sequence of the *Luciferase* gene, were amplified using PCR with the following

primers: 1) forward 5'-GTAAAATCGATAAGGATCCGTCGAC-3', (Hokkaido System Science), and 2) reverse: 5'-CAGCTGAAACTGCAGAAAGATATCAAAGAATTCTTAATCCAGATCCACAACCT TCGCTTC-3' as primers amplifying part of the vector backbone and the 5' portion of the *Luciferase* gene, and 3) forward 5'-GATATCTTTCTGCAGTTTCAGCTGCCAATCATCCAAAAAATTATTATCATGG-3', and 4) reverse 5'-CATCGGTCGACGGATCCTTATCG-3' as primers amplifying part of the vector backbone and the 3' portion of the *Luciferase* gene. Both PCR products were digested by *Pst*I and *Bam*HI, and mutually ligated. The resulting vector, which contained multiple cloning sequences (5'-TAAGAATTCTTTGATATCTTTCTGCAGTTTCAGCTG-3': Stop-*Eco*RI-*Eco*RV-*Pst*I-*Pvu*II) between the 5'- and 3'-partial *Luciferase* sequences, was designated as pGL3-SSA.

**Construction of the pSSA-Tyr-1 and pSSA-Tyr-2/3 Plasmids.**

We amplified 199-base and 200-base fragments containing the target sequences for *Tyrosinase* (Tyr-1, and both Tyr-2 and Tyr-3, respectively, **Figure S1D**) from C57BL/6 mouse genomic DNA by PCR. The PCR products were 5'-end phosphorylated with the Mighty Cloning kit (TaKaRa), and inserted into the *Eco*RV sites of the pGL3-SSA plasmid (see above). The resulting vectors were designated as pSSA-Tyr-1 and pSSA-Tyr-2/3, respectively.

**Oligonucleotide Sequences for the Target Sequences (Hokkaido System Science)**

**pSSA-Tyr-1:**

**Forward oligonucleotide:** 5'-GGCACCTATGGCCAAATGAACAATGGG-3'

**Reverse oligonucleotide:** 5'-GTTCCCACAATAACAAGAAAAGTCTGTGCC-3'

**pSSA-Tyr-2/3:**

**Forward oligonucleotide:** 5'-TGGAACAAGCCAGTCGTATCTGGCC-3'

**Reverse oligonucleotide:** 5'-TCACAGATGGCTCTGATACAGCAAGCTG-3'

**Construction of the pX330-Tyr-1, pX330-Tyr-2, pX330-Tyr-3, pX330-Bmal1-1, pX330-Bmal1-2, and pX330-Bmal1-3 Plasmids.**

Oligonucleotides (Hokkaido System Science) containing the target sequences for *Tyrosinase* and *Bmal1* (Tyr-1, Tyr-2, Tyr-3, Bmal1-1, Bmal1-2, and Bmal1-3, respectively) were annealed and inserted into the *Bbs*I sites downstream of the U6 promoter on the pX330 plasmid (Cong et al., 2013; Ran et al., 2013) [Addgene #42230]. The resulting vectors were designated as pX330-Tyr-1, pX330-Tyr-2, pX330-Tyr-3, pX330-Bmal1-1, pX330-Bmal1-2, and pX330-Bmal1-3, respectively.

**Oligonucleotide Sequences for the Target Sequences**

**Tyr-1:**

**Forward oligonucleotide:** 5'-CACCGTGTCAAGGGACACACTGCT-3'

**Reverse oligonucleotide:** 5'-AAACAGCAGTGTGTCCCTTGACAC-3'

**Tyr-2:**

**Forward oligonucleotide:** 5'-CACCGTTATTGCTGCAGCTCTCTC-3'

**Reverse oligonucleotide:** 5'-AAACGAGAGAGCTGCAGCAATAAC-3'

**Tyr-3:**

**Forward oligonucleotide:** 5'-CACCGAAGAAGAAGCAACCCCAGG-3'

**Reverse oligonucleotide:** 5'-AAACCCTGGGGTTGCTTCTTCTTC-3'

**Bmal1-1:**

**Forward oligonucleotide:** 5'-CACCGTGTGGACTGCAATCGCAAG-3'

**Reverse oligonucleotide:** 5'-AAACCTTGCGATTGCAGTCCACAC-3'

**Bmal1-2:**

**Forward oligonucleotide:** 5'-CACCGTGTTCTGCATATTCTAACC-3'

**Reverse oligonucleotide:** 5'-AAACGGTTAGAATATGCAGAACAC-3'

**Bmal1-3:**

**Forward oligonucleotide:** 5'-CACCGTCAGATTGAAAAGAGGCGT-3'

**Reverse oligonucleotide:** 5'-AAACACGCCTCTTTTCAATCTGAC-3'

**SSA Assay**

293T cells were maintained in DMEM (Life Technologies) supplemented with 10% FBS (JRH Biosciences) and antibiotics (100 U/ml penicillin and 100 µg/ml streptomycin; Life Technologies). One day prior to transfection, the cells were plated onto six-well plates at a density of $4\times10^5$ cells per well. The following day, the cells were co-transfected using FuGene6 (Roche) with 1 µg of pSSA-Tyr-1 or pSSA-Tyr-2/3 reporter plasmids in the presence of the following constructs, as

indicated in **Figure S1E**: 0 or 2 μg of pX330, pX330-Tyr-1, pX330-Tyr-2, or pX330-Tyr-3 plasmid, according to the manufacturer's instructions. Empty vector was used to bring the total amount of DNA to 3 μg per well. In addition, 50 ng of a phRL-CMV plasmid [Renilla *luciferase* (*RLuc*) reporter vector, Promega] was included in each transfection as an internal control for transfection efficiency. Forty-eight hours after transfection, the cells were harvested and assayed using the Dual-Luciferase Reporter Assay System (Promega). The Luciferase activity was normalized to the Rluc activity.

**Cas9 mRNA Synthesis**

p3s-Cas9HC plasmid(Cho et al., 2013) [Addgene #43945], which includes a T7 promoter-fused *Cas9* coding region, was digested with *Xba*I (TaKaRa), and used as the template for *in vitro* transcription using the mMESSAGE mMACHINE T7 kit (Life Technologies). The *Cas9* mRNA was purified using the MEGAclear kit (Life Technologies).

**gRNA Synthesis**

The gRNA templates for *Tyr* (**Figure 1C**) and *Bmal1* (**Figure S4A**) were simultaneously fused to the T7 promoter and amplified from the pX330-*Tyr* and pX330-*Bmal1* vectors, respectively (see above) by PCR using the primers listed below (Hokkaido System Science) (Wang et al., 2013). Alternatively, the gRNA templates for *Cry1*, *Cry2*, *Per1*, *Per2, Hcrt* (**Figures S4B, S4C and S4K**), *Nr1*, *Nr2a*, *Nr2b*, *Nr2c*, *Nr2d*, *Nr3a* (set 1 and 2), *Nr3b* (**Figures S5A-G and S6A**), and *Tyr* (**Figure 7D**) were directly synthesized and fused to the T7 promoter by PCR. First,

the partial fragments of the gRNA templates including each target sequence were amplified from pX330 plasmids (Addgene #42230) using PCR with the Common Reverse primer and Forward primer-1 (Hokkaido System Science) for each target sequence (**Table S3**). Subsequently, the T7 promoter-fused gRNA templates were amplified from the diluted PCR products using PCR with the Common Reverse primer and Forward primer-2 (Hokkaido System Science) for each target sequence (**Table S3**).

The T7 promoter-fused gRNA PCR fragments were used as the template for *in vitro* transcription using the MEGAshortscript T7 kit (Life Technologies). The gRNAs were purified using the MEGAclear kit (Life Technologies).

### Common Reverse Oligonucleotide for T7-gRNAs:

5'-AAAAGCACCGACTCGGTGCC-3' (Wang et al., 2013)

### Oligonucleotide Sequences for T7-gRNAs of *Tyr* (set 1) and *Bmal1*

**Tyr-1 Forward oligonucleotide:**

5'-GGGCCTAATACGACTCACTATAGGTGTCAAGGGACACACTGCT-3'

**Tyr-2 Forward oligonucleotide:**

5'-GGGCCTAATACGACTCACTATAGGTTATTGCTGCAGCTCTCTC-3'

**Tyr-3 Forward oligonucleotide:**

5'-GGGCCTAATACGACTCACTATAGGAAGAAGAAGCAACCCCAGG-3'

**Bmal1-1 Forward oligonucleotide:**

5'-GGGCCTAATACGACTCACTATAGGTGTGGACTGCAATCGCAAG-3'

**Bmal1-2 Forward oligonucleotide:**

5'-GGGCCTAATACGACTCACTATAGGTGTTCTGCATATTCTAACC-3'

**Bmal1-3 Forward oligonucleotide:**

5'-GGGCCTAATACGACTCACTATAGGTCAGATTGAAAAGAGGCGT-3'

Oligonucleotide Sequences for Other T7-gRNAs

Oligonucleotide sequences of triple-target gRNAs (T7-gRNAs) for *Cry1*, *Cry2*, *Per1*, *Per2*, *Hcrt, Nr1*, *Nr2a*, *Nr2b*, *Nr2c*, *Nr2d*, *Nr3a* (set 1 and 2), *Nr3b*, and *Tyr* (set 2 and 3) genes are described in **Table S3**.

**Genotyping of KO Mice by Quantitative PCR (qPCR) and Sequencing**

We first prepared the genomic DNA of wild type and *Tyr* KO mice from their brains, scalps, and tails using the Wizard Genomic DNA Purification Kit (Promega, wild type, *Tyr* KO mice, **Figure S1H**) according to the manufacturer's instructions, then performed qPCR analysis for genotyping of these mice using the ABI PRISM 7900 (Applied Biosystems)/ QuantStudio7 Real-Time PCR System (Life Technologies), SYBR Premix Ex Taq GC (TaKaRa) and primers for qPCR (**Table S4**, Hokkaido System Science) and confirmed that the quantitative qPCR results matched with each other among the genomic DNAs extracted from brains, scalps and tails. Therefore, we hereafter prepared the genomic DNA only from the tails using the DNeasy Blood & Tissue Kit (QIAGEN) for genotyping of other KO mice generated for sleep/wake phenotyping (*Bmal1*, *Cry1*/*Cry2*, *Per1*/*Per2*, *Hcrt, Nr2a*, *Nr2b*, *Nr2c*, *Nr2d*, *Nr3a*, *Nr3b* and *Tyr* KO mice). The absolute target site abundance was calculated using a

standard curve obtained from wild-type genomic DNA. The amount of *Tbp*(Tsujino et al., 2013) was quantified and used as an internal control.

When the amplified intact DNA by qPCR is less than 0.2% of wild-type genome, we judged as the target DNA is not detectable. When either three targets of the gene were not detectable, we classified the animal as a knock-out. When all three targets were detectable, genotyping by sequencing was performed. 0.6 ~ 1 kb around the each target sequence was amplified by PCR with Ex Taq (TaKaRa) and the primers (**Table S4**, Hokkaido System Science). The fragment was subcloned into pGEM-T-easy vector (Promega), and sequenced. When every subcloned sequence has deletion and/or insertion which is not an in-frame, the target was labeled as knock-out. When the target gene has at least one knocked-out target by sequence, the animal was classified as KO. Otherwise the animal was classified as non-KO. For double-KO animals, we classified the animal as KO when both genes were knocked out by the criteria written above.

**Protein Quantification**

Absolute amount of TYR and NR3A proteins were quantified by selected reaction monitoring (SRM) MS. Sample processing for the MS analysis was performed according to a phase-transfer surfactant (PTS) protocol (Masuda et al.) with several modifications. To analyze TYR abundance, ears from the mutant mice *Tyr* #3, *Tyr* #4, and *Nr3a* (set 2) # 10 were used. To analyze NR3A abundance, brains from the mutant mice *Tyr* #3, *Tyr* #4, *Nr3a* (set 1) # 1 - # 8, and *Nr3a* (set 2) # 1 - # 12 were used. In brief, the tissues were homogenized by sonication in PTS buffer (12 mM sodium deoxycholate, 12 mM sodium N-lauroylsarcosinate, and 50 mM $NH_4HCO_3$) containing a phosphatase inhibitor cocktail (Nacalai Tesque) and a protease inhibitor

cocktail (Nacalai Tesque) and were clarified by centrifugation at 10,000xg for 10 min. The resulting homogenates were frozen in liquid nitrogen and stored at -80°C until use. Protein concentrations were determined by Quick Start Bradford Dye Reagent (Bio-Rad).

As internal standards, we added the synthetic peptides with the isotope labeled lysine and arginine residue ($^{13}C_6$-Lys and $^{13}C_6{}^{15}N_4$-Arg, respectively). The synthetic peptides were pre-quantified and digested to produce specific sequences for the quantification of target proteins (DTLLGGSEIWR for the quantification of Tyr protein and VVTLIEHPFVFTR for the quantification of NR3A protein) according to our newly developed method described elsewhere. The proteins/standards mixture were subjected to cysteine reduction and alkylation (10 mM TCEP at 37°C for 1 hr and 15 mM iodoacetamide at 37°C for 30 min in dark) followed by 5-fold dilution with 50 mM $NH_4HCO_3$ solution. Then, enzymatic cleavage of proteins was performed by 8 hr-incubation with 1:50 (w/w) LysC followed by 16 hr-incubation with 1:50 (w/w) trypsin at 37°C. The digestion was stopped by mixing an equal volume of ethyl acetate in the presence of 0.5% TFA. The surfactants in the sample were removed by discarding the ethyl acetate phase. The left aqueous phase containing peptides was dried with SpeedVac (Thermo Scientific). The dried peptide mixture was then dissolved in an analytical buffer (2% acetonitrile and 0.1% TFA). The resulting peptide solution was desalted by using StageTip (Rappsilber et al.). Twenty μg of the peptide mixture prepared from brain was dissolved in 20 μL of analytical buffer. 100 μg of the peptide mixture prepared from ear was pre-fractionated into 6 fractions by StageTip-based fractionation (Wisniewski et al.), and then the fractions were dissolved in 14 - 30μL of analytical buffer.

The resulting peptide mixture corresponding to approximately 1μg of proteins was analyzed by liquid chromatography (LC)-MS using a triple quadruple mass

spectrometer (TSQ Vantage EMR mass spectrometer, Thermo Scientific) equipped with a captive spray ionization source (Michrom Bioresources), a nano-Advance UHPLC system (Bruker Daltonics), and an HTC-PAL autosampler (CTC Analytics) with a trap column (0.3 x 5 mm, L-column, ODS, Chemicals Evaluation and Research Institute, Japan). Analytical samples were separated by reversed phase chromatography, in which we used a home-made capillary column (length of 200 mm and inner diameter of 100 μm) packed with 2 μm C18 resin (L-column2, Chemicals Evaluation and Research Institute, Japan), a gradient of acetonitrile from 4 to 36% in 0.5% acetic acid over 105 min at a flow late 300 nL/min. Elution was directly electrosprayed (1.6 kV) into the MS.

To analyze TYR protein in ear samples, the heavy and light versions of DTLLGGSEIWR were monitored by LC-SRM-MS by using the SRM transitions of m/z 623.8 to 804.4 (for the light version) and m/z 628.8 to 814.4 (for the heavy version). To analyze NR3a protein in brain samples, the heavy and light versions of VVTLIEHPFVFTR were monitored by LC-SRM-MS by using the SRM transitions of m/z 520.0 to 766.4 (for the light version) and m/z 523.3 to 766.4 (for the heavy version).

**Library Preparation for Exome Sequencing**

Exome libraries were constructed using SureSelectQXT Reagent Kit (Cat. No. G9681A, Agilent Technologies) and SureSelectXT Mouse All Exon Kit V1 (Cat. No. 5190-4641, Agilent Technologies) according to the manufacturer's instructions. Fragmentation and adapter-tagging of purified genomic DNA samples were performed by transposase-based reaction. After an amplification of adapter-tagged DNA library, purification was performed with AMPure XP beads (Beckman Coulter).

The purified libraries were hybridized to the SureSelect capture library, and collected hybridized DNA using streptavidin-coated beads. The enriched DNA libraries were amplified with PCR using the appropriate pair of dual indexing primers to add index tags for the Illumina TruSeq system. In each purification step, the length distribution and concentration of DNA molecules in libraries were analyzed using the 2100 Bioanalyzer (Agilent Technologies).

**Exome Sequencing and Indel Detection**

The libraries were subjected to on-board cluster generation using TruSeq Rapid PE Cluster Kit (Cat. No. PE-402-4001) and sequenced on Rapid Run Mode of Illumina HiSeq 1500 (Illumina) to obtain paired-end reads with 126 cycles using three 50-cycle SBS kits (Cat. No. FC-402-4002), taking advantage of surplus reagents as demonstrated previously (Tatsumi K, 2015, in press.). 5% PhiX spike-in was added to each lane as control. Image analysis and base calling were executed using the standard Illumina software consisting of HiSeq Control Software (HCS) ver. 2.0.12.0 and Real-Time Analysis (RTA) ver. 1.17.21.3. Quality of the raw sequence data were controlled by FastQC ver. 0.11.1 (**http://www.bioinformatics.bbsrc.ac.uk/projects/fastqc/**). Removal of adapter sequences and low-quality reads was performed with Trim Galore ver. 0.3.3 with the parameters '-e 0.1 -q 30' (**http://www.bioinformatics.babraham.ac.uk/projects/trim_galore/**). Additionally, reads with the average per-base quality score of no more than 30 were removed with an original script. The reads filtered as above were aligned with the genome sequences GRCm38/mm10 by BWA ver. 0.7.10-r789 using the BWA-MEM algorithm (Li and Durbin, 2010). Potential PCR duplicates among the mapped paired reads

were removed using the MarkDuplicates function of Picard Tools ver. 1.122 (**http://picard.sourceforge.net/**). The sequencing statistics including the number of reads, mapping rate and exome on-bait coverages were summarized by the CalculateHsMetrics function of Picard Tools.

Local realignment of the mapped reads was performed by RealignerTargetCreator and IndelRealigner of the Genome Analysis Toolkit (GATK) package ver. 3.2-2 (McKenna et al., 2010), and recalibration based on per-base quality score were performed with the BaseRecalibrator and PrintReads functions. For these processes, the mm9-based exome region data with 100 bp padding provided by Agilent Technologies was converted to mm10 using the UCSC LiftOver program (**https://genome.ucsc.edu/util.html**) (Rhead et al., 2010), and insertion and deletion mutations (indels) from NCBI dbSNP (build 137) were used as known sites. The sample-specific indels were called using the HaplotypeCaller in GATK after applying local realignment and recalibration performed above.

SnpEff package ver. 4.0E (Cingolani et al., 2012) was used to filter and annotate the indels causing high-impact coding variants. We defined as high-impact mutations both the indels categorized in 'HIGH' by the SnpEff definition and the in-frame indels. The indels in both the samples and the control were removed, in comparison with the indels in the control. On- and off-target indels were visualized and evaluated on the UCSC Integrative Genomics Viewer (IGV) ver. 2.3.36 (Thorvaldsdottir et al., 2013).

The exome sequencing data have been deposited and are available in the DNA Data Bank of Japan (DDBJ). The accession numbers for *Tyr* KO and *Nr3a* KO data are DRA003478 and DRA003920 respectively.

**CRISPR gRNA Database Development**

The first step in automatically detecting gRNA sites was to extract candidate targets. The process is described here for a single gene, and is repeated for all genes when running the method. Using the genome annotation file and the genomic sequence, we extracted the sequence of all exons shared by all known isoforms of the gene. This was necessary to ensure that we targeted a gene, rather than only a few of its isoforms. We then extracted all the sequences that matched the [G, C, or A]$N_{20}$GG pattern and those for which the reverse-complement matched this pattern. This list represented all the possible candidates for the gene. The next steps were used to filter this list and to keep only suitable targets. Each target needed to pass all the steps, so the order did not have any impact on the selection. The steps were therefore performed in the most computationally efficient order.

The candidate gRNAs needed to target a unique site. Using Bowtie2 (Langmead and Salzberg, 2012), we eliminated all the candidates that had multiple exact matches in the genome (irrespective of location). We also removed targets with a low AT percentage (below 45%), which have a risk of binding strongly to off-target sites, and targets that contained TTTT, which tend to break the gRNA's secondary structure. Because the targets appeared in the forward primer during synthesis, we also needed to make sure they were not too similar to the reverse primer (See above "Common Reverse oligonucleotide for T7-gRNAs"). This was achieved using the Needleman-Wunsch algorithm (Needleman and Wunsch, 1970). We then used the Vienna RNA-fold package (Lorenz et al., 2011) to compute the gRNA's secondary structure. We eliminated all candidates for which the stem loop structure for Cas9 recognition could not fold (Nishimasu et al., 2014), except if the folding energy was above -18 (indicating that the 'wrong' structure was very unstable). Finally, we evaluated the off-target risk using our own implementation of the Zhang tool (Ran et

al., 2013). To ensure that all targets stored in the database were as safe as possible, we used a very strict threshold and rejected candidates with a score below 75.

Candidates that passed all the filtering steps were saved and stored in the database, which is accessible online at **http://crispr.riken.jp**.

**Statistical Analyses**

Statistical analyses were performed by Microsoft Excel or R version 3.1.0(2015).

For sleep phenotype analyses of CRISPR KO mice and conventional circadian KO mice, normality was evaluated by Kolmogorov-Smirnov test at the significance level of 0.05. The homogeneity of variance for each group was evaluated by Bartlett's test when all the member of the group was normal, or Levene's test when not. In both tests, significance level was set to 0.05. The sleep phenotype of every KO strain was compared to the control (C57BL/6N, male, n=108) by Dunnett's test when the group has homogenous variance and Dunnett's Modified Tukey-Kramer pairwise multiple comparison test when not.

The histogram at the top of each sleep/wake parameter chart (**Figures 4C, F, 5C, F, and S3M**) shows the results of C57BL/6N male mice (n = 108). The error bar is the SEM for each strain, and the black dashed vertical line and gray shaded area are the mean and 1 SD range from the recordings of C57BL/6N male mice.

To estimate the sample size for phenotype evaluation, we compared the sleep time control dataset $Xc$ (C57BL/6N, male, n=108) to a simulated dataset $Xs$ which have the same distribution except a mean of 1 SD (50.8 min) less or much than control ($\widetilde{Xs} = \widetilde{Xc} \pm 50.8$). We randomly sampled $k$ ($2 \leq k \leq 20$) data from $Xs$ and compared with $Xc$ by Dunnett's test with the significance level of 0.05. This test was

repeated 1000 times for one $k$. We calculated the rate of $p < 0.05$ as sensitivity for each $k$ from 2 to 20. According to this calculation, we found that the sample size $k \geq 2$ provides more than 25% sensitivity whereas the sample size $k \geq 6$ provides more than 50% sensitivity. In this study, we selected the sample size $k \geq 8$ to achieve more than 75% sensitivity for the CRISPR knockout study of NMDA receptor family members.

For pharmacological studies, means of two sets of data were evaluated. First, the normality was tested by Shapiro-Wilk test at the significant level of 0.05. When the normality is confirmed in both groups, the homogeneity of variance was tested by *F*-test at the significance level of 0.05. When two groups were normal distributions with equal variance, Student's *t*-test, when the groups are normal distributions without equal variance, Welch's *t*-test, otherwise two-sample Wilcoxon test was applied.

For the sleep time evaluation of *Nr3a* KO mice by EEG/EMG, daily sleep time was compared between *Nr3a* KO group (n=2) and wild type group (n=6). The normality for wild type group was tested by Shapiro-Wilk test at the significance level of 0.05 and turned out to be normal ($p = 0.9195$). Since there were only two mice tested in the *Nr3a* KO group, they were estimated to be a normal distribution because of normality confirmed in other EEG recording done in this study (the Shapiro-Wilk test for wild-type, DZP-control group, DZP-treated group, MAP-control group and MAP-treated group were 0.6609, 0.1003, 0.4282, 0.4709 and 0.3382, respectively). *F*-test at the significance level of 0.05 showed these groups do not have different variance ($p = 0.3014$). Therefore, the mean sleep time was tested by Student's *t*-test ($p = 0.0201$, **Figure S6E**).

The i.p. injection was performed blindly without informing the injector the content of the drug. Randomization was not performed for processing data.

In this study, $p < 0.05$ was considered as significant (*$p < 0.05$, **$p < 0.01$, ***$p < 0.001$ and n.s. for not significant evaluations).

# SUPPLEMENTAL DATA

**Figure S1. A triple-target CRISPR method for highly efficient production of whole-body biallelic KO mice, Related to Figure 1.**

(A) Computational simulation predicting how efficiently one or more alleles are cut out when different numbers of gRNAs are used for the same target gene. Knockout efficiency was calculated for an increasing number of target alleles: single gene mono-allelic (one allele), single gene biallelic (two alleles), double gene biallelic (four alleles), and triple gene biallelic KO (six alleles). In each simulation, we compared single- (one target per gene), dual- (two targets), triple- (three targets), sextuple- (six targets), and decuple- (ten targets) target methods. Each method uses the same amount of total gRNA. A computational model of the different methods (except the single-target method) predicts the minimum efficiency.

(B) Distribution of the gRNA dissociation constant ($K$) used in the computational simulation of CRISPR-based KO (**Figure S1A**). Distribution of the gRNA dissociation constant ($K$) follows the log-normal distribution with its geometric mean and geometric standard deviation as 1.0 and 2.5, respectively. Without loss of generality, we can use 1.0 for the geometric mean in the log-normal distribution of the gRNA dissociation constant. We then estimated three gRNA dissociation constants from the SSA assay for three gRNAs for *Tyr* gene ($K_1$ = 2.32203, $K_2$ = 1.16562 and $K_3$ = 0.369466, **Figure 1D**). Since the geometric standard deviation of these values was 2.53097, we used 2.5 for the geometric standard deviation in the log-normal distribution of the gRNA dissociation constant.

(C) Computer simulation predicting the minimum efficiency (mean ± SD) of single-gene biallelic KO with different recovery rates of mutations ($\alpha$ = 0.05, 0.10 and

0.15) and total gRNA concentrations ($S$ = 5, 10 and 15). We note that total gRNA concentration ($S$) is a relative value to the geometric mean of gRNA dissociation constants (1.0).

(D) Sequences of the inserted fragment for the SSA assay of gRNAs for the *Tyr* gene. The fragment sequences for the SSA vector are shown with three target sequences (blue, orange, and green) for Tyr-1, Tyr-2 and Tyr-3 gRNAs, respectively. Mouse genomic sequence data were obtained from GRCm38/mm10 via the UCSC Genome Browser (**http://genome.ucsc.edu/**) (Rhead et al., 2010).

(E) Schematic diagram of the single-strand annealing (SSA) assay. The SSA-reporter vector contained 5' and 3' *Luciferase* gene fragments that shared 702 bp of direct repeats. These fragments were separated by stop codon and gRNA target site. A gRNA/Cas9-mediated double-strand break at the target site induced an SSA reaction between the homologous regions, producing an active *Luciferase* gene.

(F) Computational simulation with estimated values for a recovery rate of mutation ($\alpha$ = 0.136) and total gRNA concentration ($S$ = 5.72) predicting how efficiently two alleles of a gene are cut out when single or triple gRNAs are used for the same target gene. We first constructed three single-target CRISPR models with three different dissociation constants ($K_1$ = 2.32203, $K_2$ = 1.16562 and $K_3$ = 0.369466) estimated from the SSA assay results for Tyr-1, Tyr-2, and Tyr-3, respectively. We note that estimated values of dissociation constants ($K_1$, $K_2$ and $K_3$) are inverse proportional to the DNA-cleavage efficiency in SSA assay, and geometric mean of dissociation constants is set to be 1.0 without loss of generality. The single-target CRISPR efficiencies of the experiments are shown in blue, orange and green solid circles for Tyr-1 (36.0%), Tyr-2 (54.2%) and Tyr-3 (64.7%), respectively. We then compared the single-target CRISPR models and experiments to estimate the values for a recovery

rate of mutation ($\alpha$ = 0.136), total gRNA concentration ($S$ = 5.72) by least squares method. The triple-target CRISPR efficiencies of the experiment (97.5%) and simulation (82.6%) are shown in solid and open circles (red), respectively.

(G) Coat color of the *Tyr* KO mice generated with three different single-target gRNAs. See also **Figure 1E**.

(H) The genotyping of *Tyr* KO mice. The relative amount of intact DNA for each target sequence was measured by quantitative PCR (qPCR). The genomic DNA was purified from the brain, scalp and tail of each mouse. The relative amount of intact DNA for each target sequence was scaled so that the level in one wild-type mouse was defined as 100%.

(I) An MS analysis of Tyr protein in mice skin. Mass spectrometric signals obtained by monitoring a tryptic peptide of Tyr protein (upper) in *Nr3a* (set 2) #10 (**Figure S6B**), *Tyr* #3 and #4 (**Figure S4D**) in the presence of isotopically labeled internal standard (lower) are shown. The peptide was absolutely quantified using a triple quadruple mass spectrometer (TSQ Vantage EMR mass spectrometer, Thermo Scientific). The peptide concentration, which represents the Tyr protein concentration, was determined to be 1.7 atmol/μg in *Nr3a* (set 2) #10, whereas the peak was not observed in *Tyr* #3 and #4.

**Figure S2. The Snappy Sleep Stager (SSS) enables non-invasive, fully automated, high-performance sleep/wake phenotyping, Related to Figure 3.**

(A) Representative wave patterns of EEG, EMG, and the pressure change in the SSS chamber, reflecting the animal's respiration flow, during NREM sleep, REM sleep, and wake states in the mouse. During NREM sleep, the respiration rate was slow and its period was stable, whereas during waking, the respiration rate was faster and its period and amplitude fluctuated more.

(B) Schematic diagram of the SSS annotation pipeline. After the mouse is set in the chamber and the respiration flow recording started, no subjective decision is necessary until the sleep staging finishes. The recorded respiration flow is sampled at 250 Hz, then digitized, and stored in a computer. The recorded data are divided into 8-second epochs. Each epoch is transformed to a power spectrum, and its characters extracted by principal component analysis. The top three principal components are used as characters, and time-series of the characters are automatically clustered by probability density clustering. Finally, the clusters are annotated as sleep or awake based on their characteristics. See **Supplemental Experimental Procedures** for detail.

(C) Sleep/wake phenotyping using simultaneously recorded EEG/EMG and respiration. Three animals were used to estimate the SSS performance. Top row shows the principal components from the SSS analysis. Bottom row shows the time course of sleep time (per hour) determined by both EEG/EMG based staging (black line) and SSS results (red line). Note that even in different individuals, the first and second principal components clearly formed two clusters. Choosing which cluster was awake state and which was sleep state was simpler than judging all of the epoch's states in conventional analyses.

(D) Accuracy of the SSS for different levels of wakefulness. Each awake epoch was categorized as “quiet awake”, “normal awake”, or “active awake”, which were defined as 0 to 33.3%, 33.3 to 66.6%, and 66.6 to 100% EMG power, respectively. Upper panel shows representative “quiet awake” and “active awake” recordings. Lower panel shows the accuracy of the SSS results for each level of wakefulness. Note that even in “quiet awake” state the accuracy exceeded 90%.

(E) Distribution of sleep/wake parameters recorded in C57BL/6J male and female mice and C57BL/6N female mice. The upper, middle and the lower rows show the data of C57BL/6J male (n = 178), C57BL/6N female (n = 72) and C57BL/6N male (n = 173) mice, respectively. The C57BL/6J male mice slept 699.3 ± 49.6 min (mean ± SD, n = 178, 7.1% CV), which is 35 minutes less than the daily sleep time of C57BL/6N mice. In females, C57BL/6N and C57BL/6J showed 636.4 ± 57.7 min and 613.2 ± 50.1 min, respectively. They had shorter sleep time than males, which presumably is an effect of the estrus cycle. The pink and sky blue dashed lines show the mean and the mean ± SD. See **Table S1**.

**Figure S3. SSS can detect various sleep/wake phenotypes, Related to Figure 4.**

(A) SSS detected the sleep-time reduction induced by a single i.p. administration of methamphetamine (MAP) at ZT2. Heatmaps show the sleep time (per hour) for all mice used in this experiment. The MAP group (n = 6) received 3 mg/kg of MAP i.p. on ZT2 of the second day, and the control group (n = 6) received vehicle i.p. at the same time. The MAP group showed less sleep than the control group for the first 3 hr after i.p. injection. Red bar at the top of the plot shows the period used for comparing the parameters in **Figure S3B**.

(B) MAP reduced the sleep time and $P_{ws}$ significantly for the following 3 hr (ZT2 to 4) after the i.p. injection of MAP. (Left) Average sleep time. (Middle and right) Average $P_{ws}$ and $P_{sw}$. Error bars represent SEM (n = 6 for each group). Welch's two sample *t*-test.

(C) A single i.p. administration of MAP reduced sleep. Plot shows the average sleep time for the MAP and control groups over time. Red bar at top indicates the 3-hr period used for comparing the groups in **Figure S3B**.

(D) SSS detects the sleep-time increase caused by a single i.p. injection of diazepam (DZP) at ZT13. Heatmaps show the sleep time (per hour) of six mice from the DZP group and the control group. The DZP group received 5 mg/kg of DZP i.p. on ZT13 of the second day, while the control group received vehicle i.p. at the same time. The DZP group showed increased sleep time for the first 5 hr after i.p. injection. Red bar at the top of the plot shows the period used for comparing the parameters in **Figure S3E**.

(E) DZP increased the sleep time and $P_{ws}$ significantly during the 5 hr (ZT13 to 17) after i.p. administration. (Left) Total sleep time. (Middle and right) Average $P_{ws}$ and

$P_{sw}$. Error bars represent SEM (n = 6 for each group). Student's *t*-test or two-sample Wilcoxon test.

(F) A single i.p. administration of DZP increased sleep. Plot shows the average sleep time for the DZP and control groups. Red bar at top indicates the 5-hr period used for comparing the groups in **Figure S3E**.

(G) After DZP increased the sleep time significantly during the first 5 hr (ZT13 to 17), DZP conversely decreased the sleep time during the second 5 hr (ZT18 to 22) after i.p. administration. (Left) Total sleep time ($p < 0.05$). (Middle and right) average $P_{ws}$ and $P_{sw}$. Error bars represent SEM (n = 6 for each group). Student's *t*-test, Welch's *t*-test or two-sample Wilcoxon test.

(H) Performance of SSS during MAP induced sleep decrease. When 3 mg/kg of MAP i.p. was given on ZT2, the accuracy, sleep sensitivity, sleep specificity, wake sensitivity and wake specificity against EEG derived sleep status were over 90%. Error bars represent SEM (n = 4 for each group). The light and dark blue bars show the saline and MAP administered group respectively. The dashed line denotes 90%.

(I) Performance of SSS during DZP induced sleep increase. When 5 mg/kg of DZP i.p. was given on ZT13, the accuracy, sleep sensitivity, sleep specificity, wake sensitivity and wake specificity against EEG derived sleep status were over 90%. Error bars represent SEM (n = 4 for each group). The light and dark blue bars show the saline and DZP administered group respectively. The dashed line denotes 90%.

(J) Sleep time of circadian-clock mutants evaluated by SSS. Altered sleep/wake phenotypes were detected in circadian-clock mutants. Heatmaps show the sleep time (per hour) for a week under light/dark conditions for C57BL/6N (n = 108), *Bmal1* KO

mice (n = 34), *Cry1*/*Cry2* double-KO mice (n = 27) and *Per1*/*Per2* double-KO mice (n = 26), respectively.

(K) Sleep time (per hour) over 24 hr averaged over six days in circadian-clock mutants. Red lines show the mean sleep time at each time of day for the mutants. Gray line shows the data for C57BL/6N male mice (n = 108). The shaded area around the line is the SEM for each time point.

(L) Averaged $P_{ws}$ and $P_{sw}$ over the course of one day in circadian-clock mutants. Red lines represent the mean transition probabilities at each time of day for the mutant strains. Gray line shows the results for C57BL/6N male mice (n = 108).

(M) Distributions of sleep/wake parameters for circadian-clock mutants. Dunnett's test or Dunnett's modified Tukey-Kramer pairwise multiple comparison test compared to C57BL/6N male mice. See also **Table S1**.

**Figure S4. Combined use of a triple-target CRISPR and SSS enables sleep/wake phenotyping in single- and double-knockout mice, Related to Figure 4.**

(A-C) Target sequences of the gRNAs for knocking out clock genes. *Bmal1* (A), *Cry1* (B, left), *Cry2* (B, right), *Per1* (C, left), and *Per2* (C, right); each gene had three target sequences. Mouse genomic sequence data were obtained from GRCm38/mm10 via the UCSC Genome Browser (**http://genome.ucsc.edu/**) (Rhead et al., 2010). The colored letters (blue, orange, and green) show the 20-base target sequences. The target sequences were designed on the sense (+) or the antisense (-) strand of genomic DNA.

(D-G) The genotype of *Tyr* KO and clock KO mice. *Tyr* (D), *Bmal1* (E), *Cry1*/*Cry2* (f) and *Per1*/*Per2* (G); each gene had three targets. The relative amount of intact DNA for each target sequence was measured by quantitative PCR (qPCR). The genomic DNA was purified from the tail of each mouse. The relative amount of intact DNA for each target sequence was scaled so that the level in a wild-type mouse was defined as 100%. The numbers and wt below the bar plot denotes the mouse id and the wild-type mouse, respectively. Genotyping by sequencing was done for three *Tyr* KO mouse (D) and *Per2* gene of one *Per1*/*Per2* KO mice (G). The sequences of mutant alleles are shown. The target sites are colored and underlined. The mutations are labeled in red. Red texts show the description of the sequence with the number of detected allele in parentheses.

(H) Average time course of the $P_{ws}$ and $P_{sw}$ for *Tyr* KO and circadian-clock mutants. Red lines and red shaded area represent the mean and SEM of the transition probabilities for each time of day for the mutants. Gray line shows the results of C57BL/6N male mice (n = 108).

(I) Sleep time (per hour) phenotype under constant darkness for individual mice in circadian mutants produced by triple-target CRISPR. Sleep-time phenotype over six days is shown for the three circadian-clock mutant mice, *Bmal1* KO mice (n = 6), *Cry1*/*Cry2* (n = 5) and *Per1*/*Per2* KO mice (n = 2).

(J) Sleep time (per hour) under constant darkness over 24 hr averaged over six days in circadian mutants produced by triple-target CRISPR. Red lines and red shaded area represent the mean and SEM of sleep time at each time of day for each strain. The light gray and black bar written at the bottom of the panel denotes the subjective time of the animal.

(K) Target sequences of the gRNAs for knocking out *Hcrt* gene. Mouse genomic sequence data were obtained from GRCm38/mm10 via the UCSC Genome Browser (**http://genome.ucsc.edu/**) (Rhead et al., 2010). The colored letters (blue, orange, and green) show the 20-base target sequences. The target sequences were designed on the sense (+) or the antisense (-) strand of genomic DNA.

(L) The genotype of *Hcrt* KO mice. The relative amount of intact DNA for each target sequence was measured by qPCR. The genomic DNA was purified from the tail of each mouse. The relative amount of intact DNA for each target sequence was scaled so that the level in a wild-type mouse was defined as 100%. The numbers and wt below the bar plot denotes the mouse id and the wild-type mouse, respectively.

(M) Average time course of the $P_{ws}$ and $P_{sw}$ for *Hcrt* KO mice. Red lines and red shaded area represent the mean and SEM of the transition probabilities for each time of day for the mutants. Gray line shows the results of C57BL/6N male mice (n = 108).

**Figure S5. Reverse genetics without crossing revealed *Nr3a* mutant to be a short-sleeper, Related to Figure 5.**

(A-G) Target sequences of the gRNAs for the knockout of NMDA receptor family. *Nr1* (A), *Nr2a* (B), *Nr2b* (C), *Nr2c* (D), *Nr2d* (E), *Nr3a* (F), and *Nr3b* (G); each had three target sequences. The mouse genomic sequence data were obtained from GRCm38/mm10 via the UCSC Genome Browser (**http://genome.ucsc.edu/**) (Rhead et al., 2010). The colored letters (blue, orange, and green) show the 20-base target sequences. The target sequences were designed on the sense or antisense strand of genomic DNA.

(H-L) The genotype of NMDA receptor family KO mice. *Nr2a* (H), *Nr2c* (I), *Nr2d* (J), *Nr3a* (set 1) (K), and *Nr3b* (L); each had three targets. The relative amount of intact DNA for each target sequence was measured by quantitative PCR (qPCR). The genomic DNA was purified from the tail of each mouse. The relative amount of intact DNA for each target sequence was scaled so that the level in a wild-type mouse was defined as 100%. The numbers and wt below the bar plot denotes the mouse id and the wild-type mouse, respectively. Genotyping by sequencing was done for one *Nr3a* KO mouse (K) and one *Nr3b* KO mice (L). The sequences of mutant alleles are shown. The target sites are colored and underlined. The mutations are labeled in red. Red texts show the description of the sequence with the number of detected allele in parentheses.

(M) Average time course of the $P_{ws}$ and $P_{sw}$ of the NMDA receptor family systematic KOs for one day. Red lines and red shaded area in each chart represent the mean and SEM of the $P_{ws}$ or $P_{sw}$ for each time of day for the mutants. Gray line shows the results of C57BL/6N male mice (n = 108).

**Figure S6. *Nr3a* mutant is a short-sleeper in multiple KO strains and in conventional sleep analysis, Related to Figure 5.**

(A) The second set of target sequences of the gRNAs for knocking out *Nr3a* gene. Note that these sequences are distinct from set 1 sequences (**Figure S5F**). Mouse genomic sequence data were obtained from GRCm38/mm10 via the UCSC Genome Browser (**http://genome.ucsc.edu/**) (Rhead et al., 2010). The colored letters (blue, orange, and green) show the 20-base target sequences. The target sequences were designed on the sense (+) or the antisense (-) strand of genomic DNA.

(B) The genotype of *Nr3a* (set 2) KO mice. The relative amount of intact DNA for each target sequence was measured by quantitative PCR (qPCR). The genomic DNA was purified from the tail of each mouse. The relative amount of intact DNA for each target sequence was scaled so that the level in a wild-type mouse was defined as 100%. The numbers and wt below the bar plot denotes the mouse id and the wild-type mouse, respectively.

(C) Average time course of the $P_{ws}$ and $P_{sw}$ for *Nr3a* KO mice (set 2). Red lines and red shaded area represent the mean and SEM of the transition probabilities for each time of day for the mutants. Gray line shows the results of C57BL/6N male mice (n = 108).

(D) The genotype of *Nr3a* (set 1) KO mice used for EEG/EMG analysis. The relative amount of intact DNA for each target sequence was measured by qPCR. The genomic DNA was purified from the tail of each mouse. The relative amount of intact DNA for each target sequence was scaled so that the level in a wild-type mouse was defined as 100%. The numbers and wt below the bar plot denotes the mouse id and the wild-type mouse, respectively.

(E) The sleep time of *Nr3a* (set 1) KO evaluated by EEG/EMG based sleep staging. *Nr3a* KO group (n = 2) showed a significant short-sleeper phenotype ($p$ = 0.02005, Student's $t$-test) than the wild-type group (n = 6). Error bars represent SEM.

(F) Mass spectrometric signals obtained by monitoring a tryptic peptide of Nr3a protein (upper) in each strain in the presence of isotopically labeled internal standard (lower) are shown. The peptide was absolutely quantified using a triple quadruple mass spectrometer (TSQ Vantage EMR mass spectrometer, Thermo Scientific). The peptide concentrations, which represents the Nr3a protein concentrations, were determined to be 2.2 atmol/μg in *Tyr* KO #3 and 5.7 atmol/μg in *Tyr* KO #4, whereas the peak was not observed in any *Nr3a* KO mice.

**Figure S7. Exome analysis of whole-body biallelic *Nr3a* (set 2) KO mice produced by triple-target CRISPR method, Related to Figure 6.**

(A) The genomic regions targeted by the three gRNAs were shown for two mice in *Nr3a* (set 2) KO group (**Figure S6B**). The upper part of each panel shows read coverage, and the lower part shows read alignments (rectangles). Horizontal lines between rectangles indicate read pairing. Different types of mutations occurring at the target sites are highlighted as follows: inter-exon deletion (red rectangles); intra-exon deletion mutation (green rectangles); short deletion (red dots); and short insertion (blue dots).

(B) Enlarged View of Read Coverage of Exome Sequence of Nr3a KO. Diminished depth shows a deletion mutation with the most severely affected site pointed by a red arrow. A blue vertical bar indicates an insertion mutation whose proportion is shown by its length. Percentages in parentheses are the proportions of indel mutations that can cause loss of gene function.

# SUPPLEMENTAL REFERENCES


Cho, S.W., Kim, S., Kim, J.M., and Kim, J.-S. (2013). Targeted genome engineering in human cells with the Cas9 RNA-guided endonuclease. Nature biotechnology *31*, 230-232.

Cingolani, P., Platts, A., Wang le, L., Coon, M., Nguyen, T., Wang, L., Land, S.J., Lu, X., and Ruden, D.M. (2012). A program for annotating and predicting the effects of single nucleotide polymorphisms, SnpEff: SNPs in the genome of Drosophila melanogaster strain w1118; iso-2; iso-3. Fly *6*, 80-92.

Cong, L., Ran, F.A., Cox, D., Lin, S., Barretto, R., Habib, N., Hsu, P.D., Wu, X., Jiang, W., Marraffini, L.a*., et al.* (2013). Multiplex genome engineering using CRISPR/Cas systems. Science (New York, NY) *339*, 819-823.

Diniz Behn, C.G., and Booth, V. (2011). Modeling the temporal architecture of rat sleep-wake behavior. Conference proceedings : Annual International Conference of the IEEE Engineering in Medicine and Biology Society IEEE Engineering in Medicine and Biology Society Conference *2011*, 4713-4716.

Langmead, B., and Salzberg, S.L. (2012). Fast gapped-read alignment with Bowtie 2. Nature methods *9*, 357-359.

Li, H., and Durbin, R. (2010). Fast and accurate long-read alignment with Burrows-Wheeler transform. Bioinformatics *26*, 589-595.

Lorenz, R., Bernhart, S.H., Honer Zu Siederdissen, C., Tafer, H., Flamm, C., Stadler, P.F., and Hofacker, I.L. (2011). ViennaRNA Package 2.0. Algorithms for molecular biology : AMB *6*, 26.

Masuda, T., Tomita, M., and Ishihama, Y. (2008). Phase transfer surfactant-aided trypsin digestion for membrane proteome analysis. J Proteome Res *7*, 731-740.

McKenna, A., Hanna, M., Banks, E., Sivachenko, A., Cibulskis, K., Kernytsky, A., Garimella, K., Altshuler, D., Gabriel, S., Daly, M*., et al.* (2010). The Genome Analysis

Toolkit: a MapReduce framework for analyzing next-generation DNA sequencing data. Genome research *20*, 1297-1303.

Needleman, S.B., and Wunsch, C.D. (1970). A general method applicable to the search for similarities in the amino acid sequence of two proteins. Journal of molecular biology *48*, 443-453.

Nishimasu, H., Ran, F.A., Hsu, P.D., Konermann, S., Shehata, S.I., Dohmae, N., Ishitani, R., Zhang, F., and Nureki, O. (2014). Crystal structure of Cas9 in complex with guide RNA and target DNA. Cell *156*, 935-949.

R core team (2015). R: A Language and Environment for Statistical Computing, R.C. Team, ed. (Vienna, Austria: R Foundation for Statistical Computing).

Rappsilber, J., Mann, M., and Ishihama, Y. (2007). Protocol for micro-purification, enrichment, pre-fractionation and storage of peptides for proteomics using StageTips. Nature protocols *2*, 1896-1906.

Tatsumi K, N.O., Itomi K, Tanegashima C, Kuraku S (2015, in press.). Optimization and cost-saving in tagmentation-based mate-pair library preparation and sequencing. Biotechniques.

Thorvaldsdottir, H., Robinson, J.T., and Mesirov, J.P. (2013). Integrative Genomics Viewer (IGV): high-performance genomics data visualization and exploration. Briefings in bioinformatics *14*, 178-192.

Tsujino, K., Narumi, R., Masumoto, K.H., Susaki, E.A., Shinohara, Y., Abe, T., Iigo, M., Wada, A., Nagano, M., Shigeyoshi, Y.*, et al.* (2013). Establishment of TSH beta real-time monitoring system in mammalian photoperiodism. Genes to cells : devoted to molecular & cellular mechanisms *18*, 575-588.

Wisniewski, J.R., Zougman, A., and Mann, M. (2009). Combination of FASP and StageTip-based fractionation allows in-depth analysis of the hippocampal membrane proteome. J Proteome Res *8*, 5674-5678.

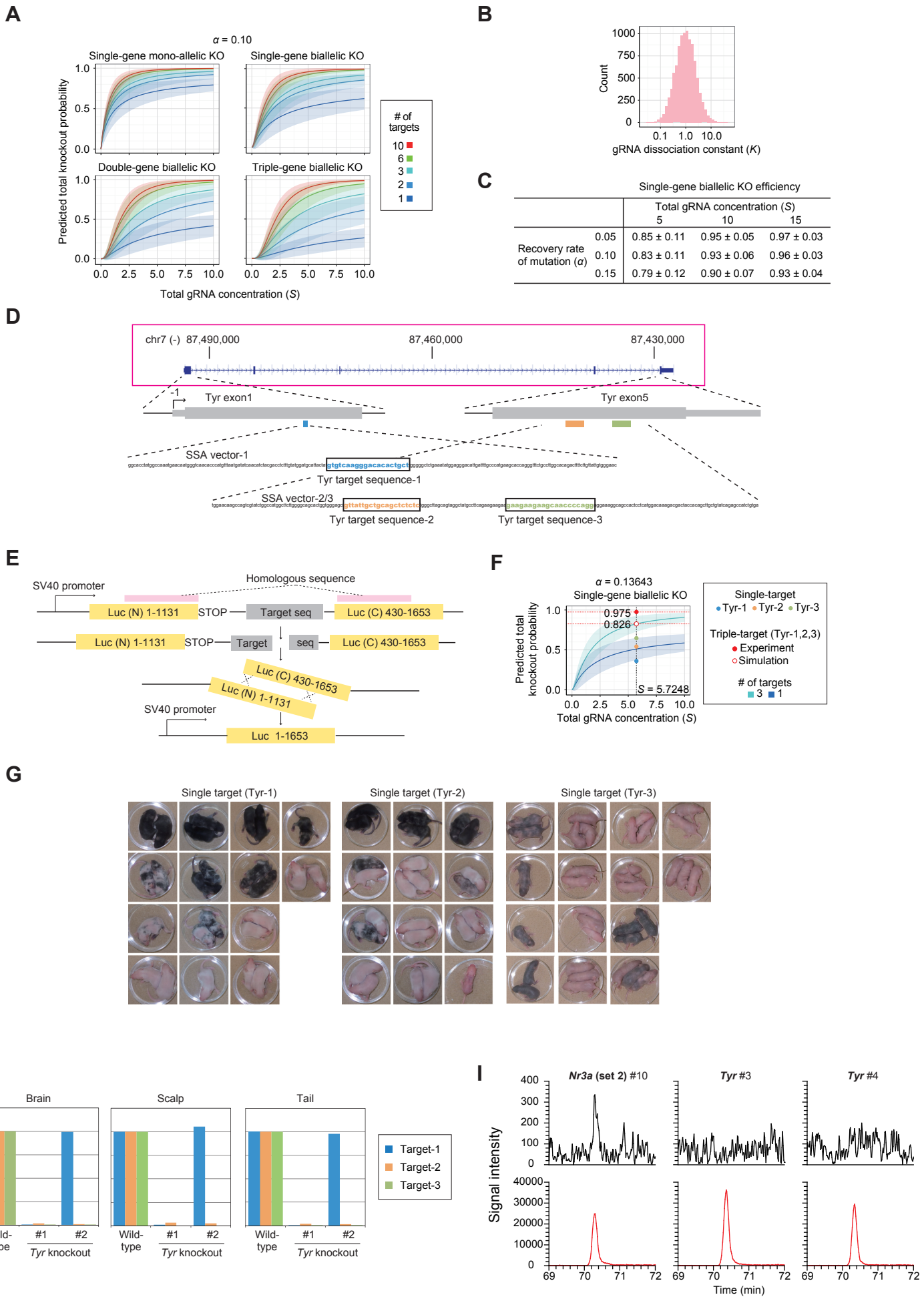


Figure S1 G.A. Sunagawa

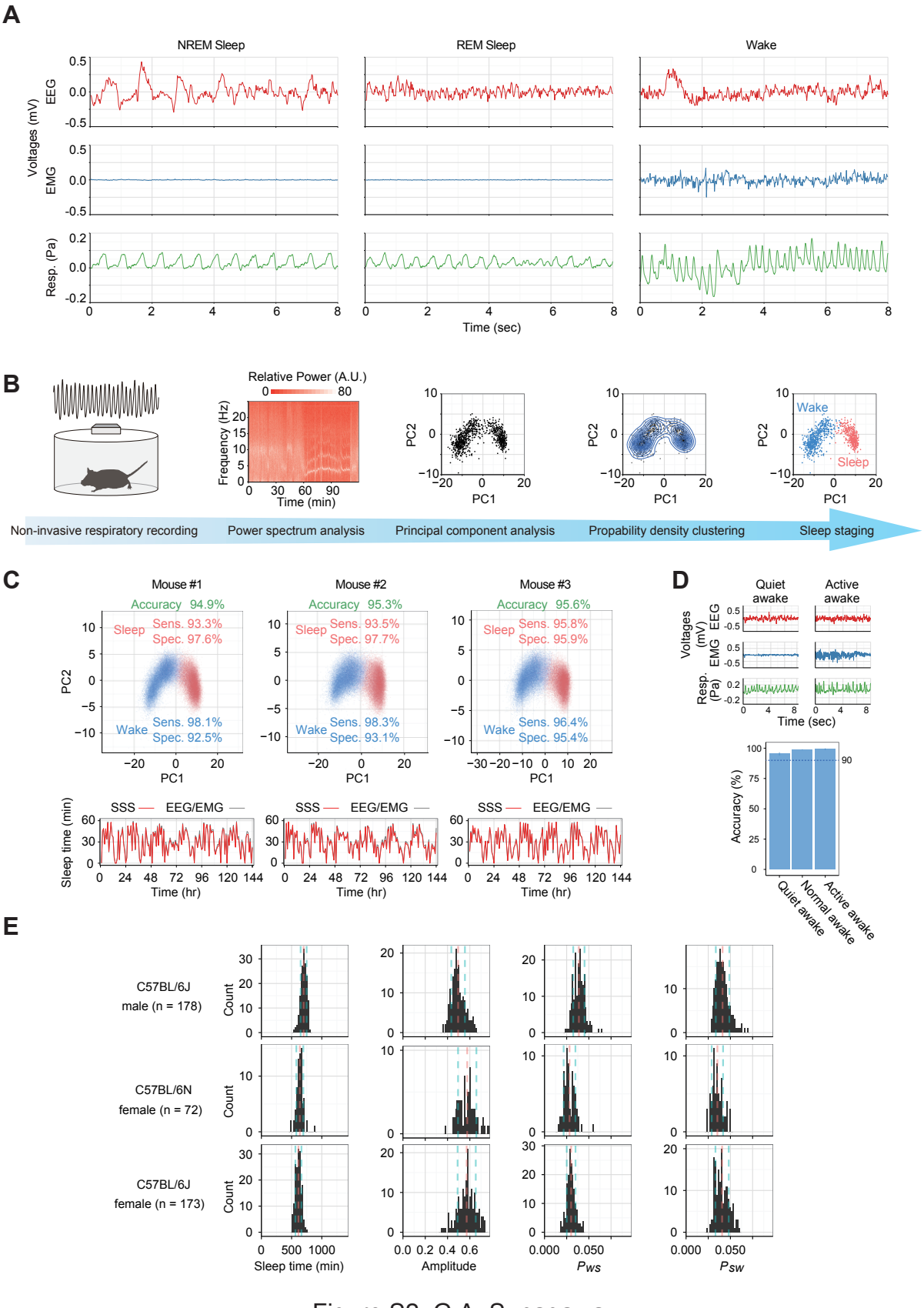


Figure S2 G.A. Sunagawa

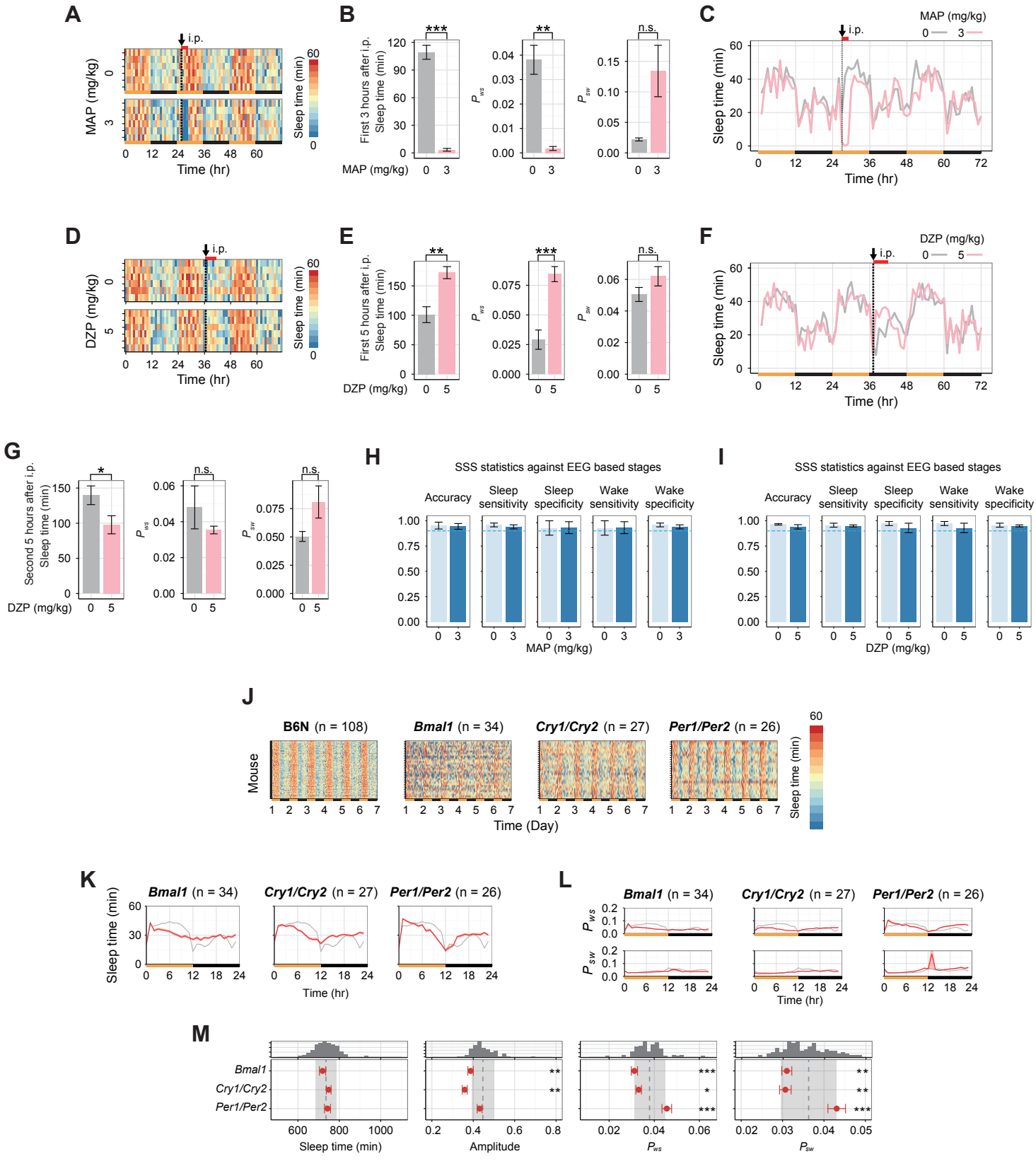


Figure S3 G.A. Sunagawa

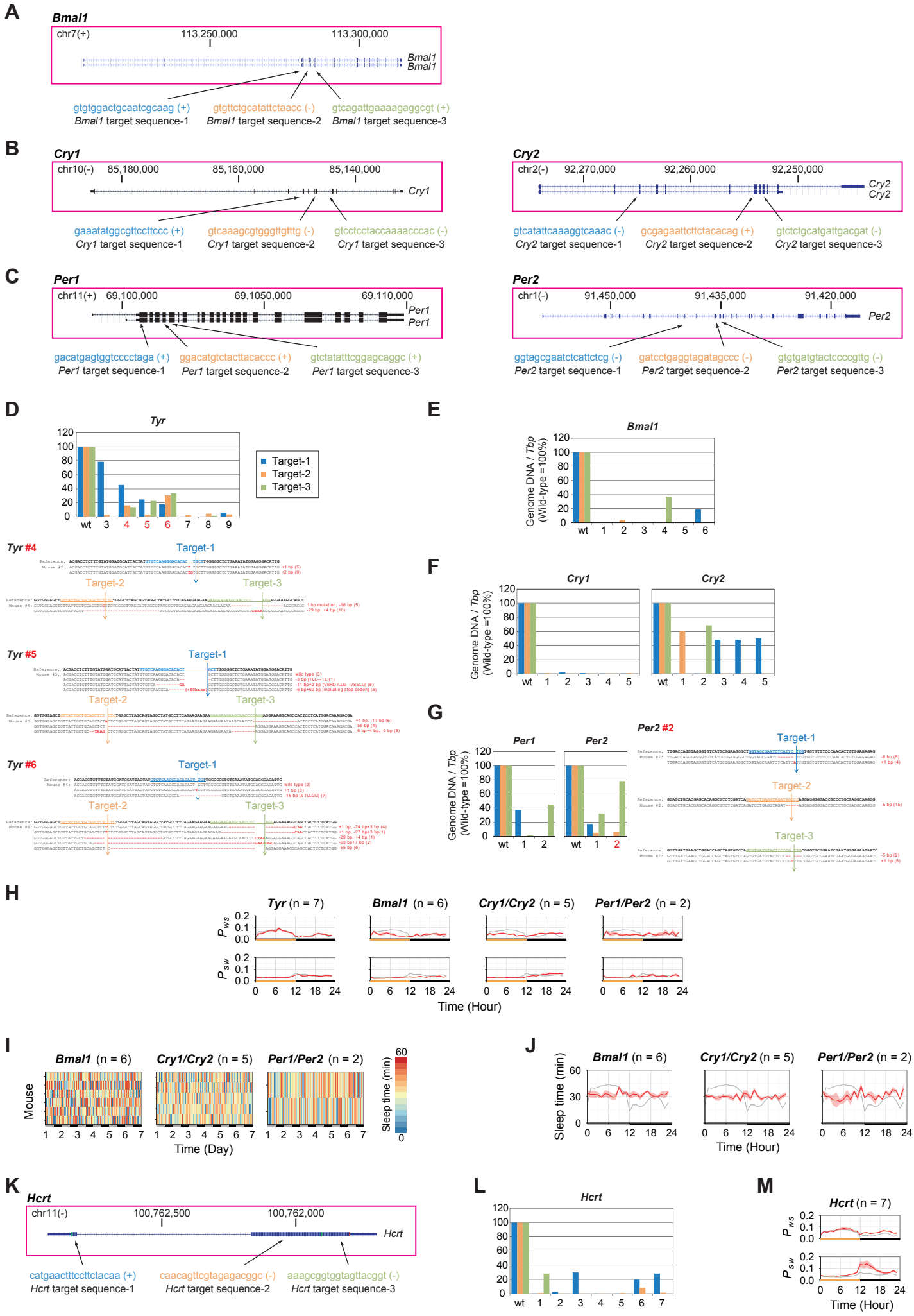


Figure S4 G.A. Sunagawa

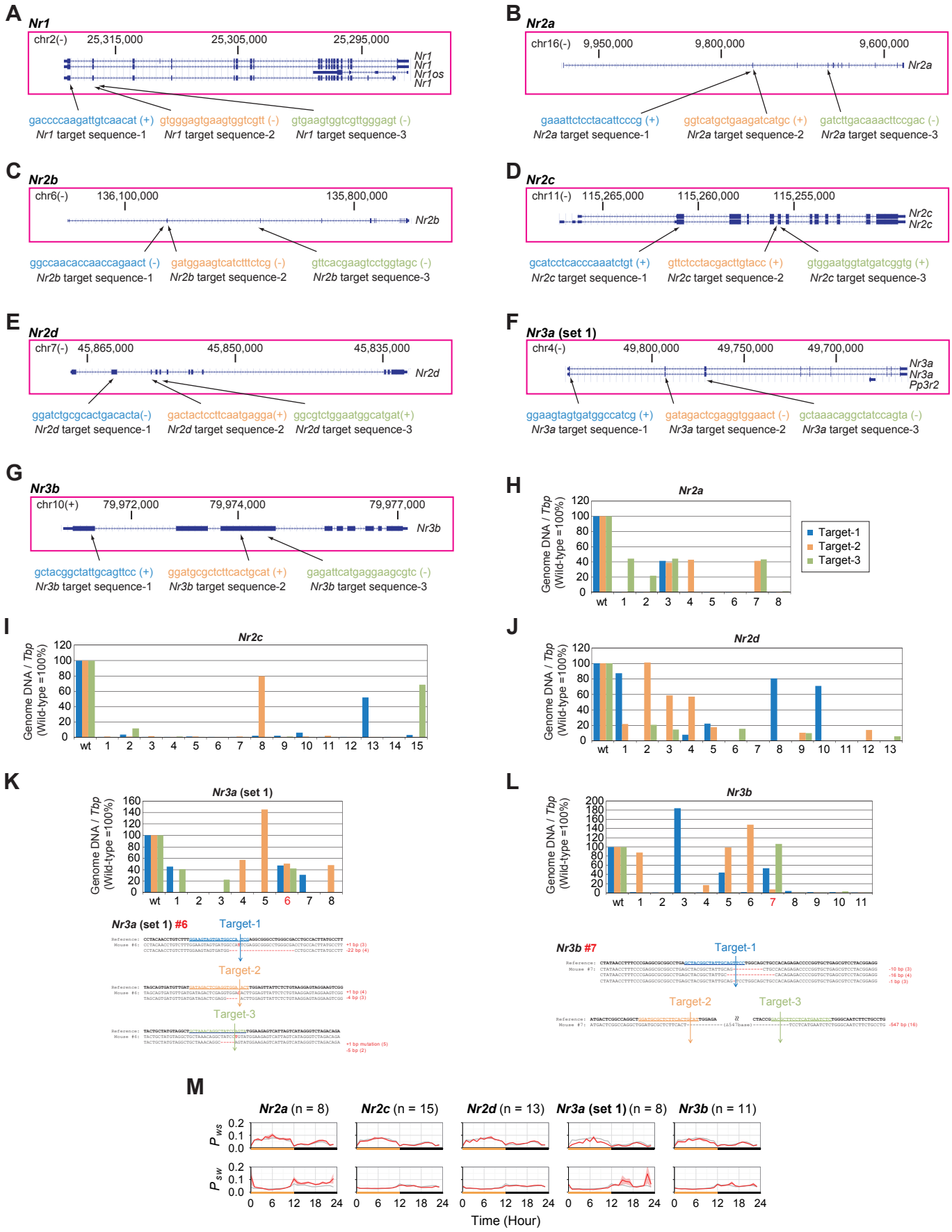


Figure S5 G.A. Sunagawa

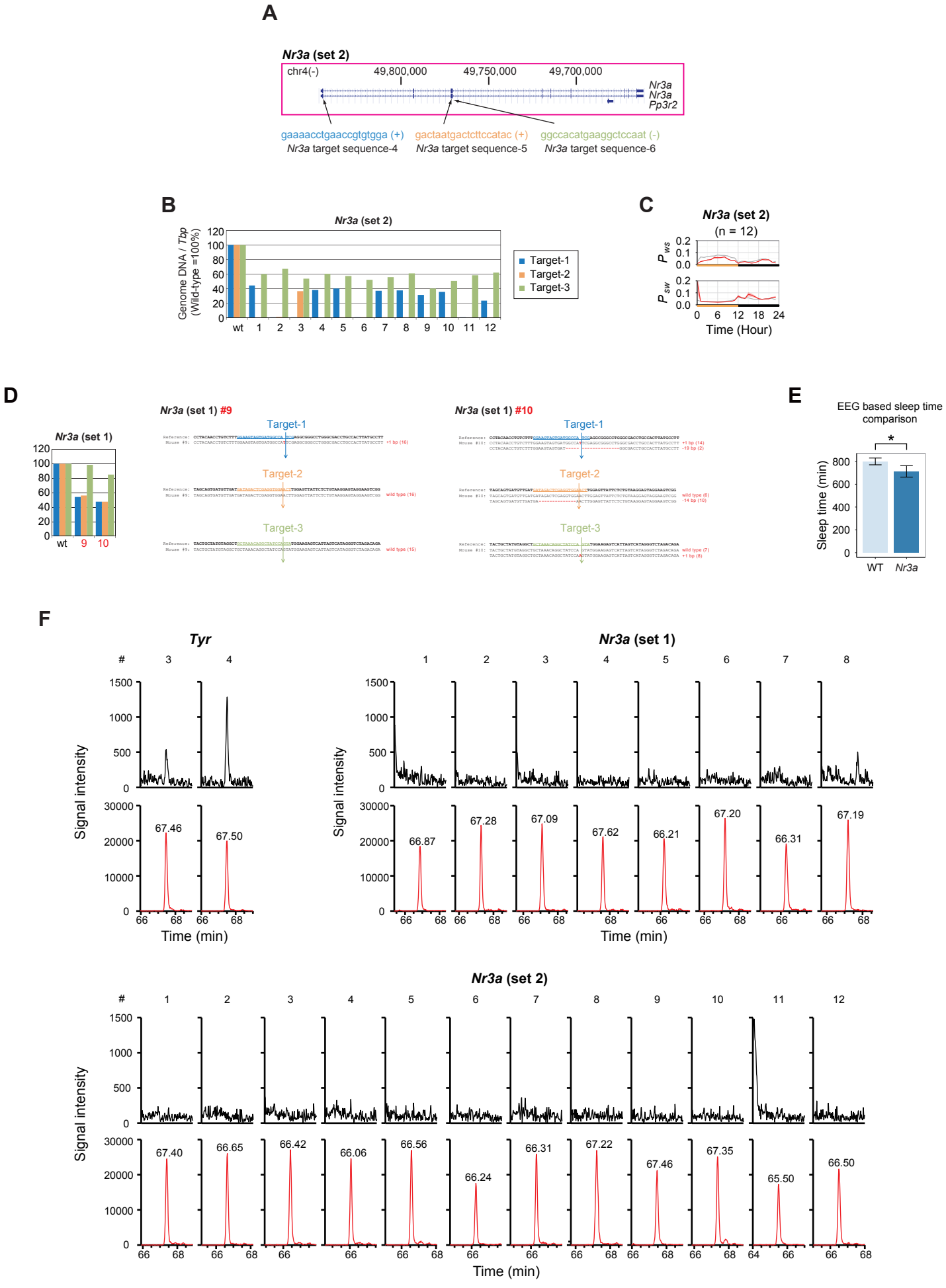


Figure S6 G.A. Sunagawa

A

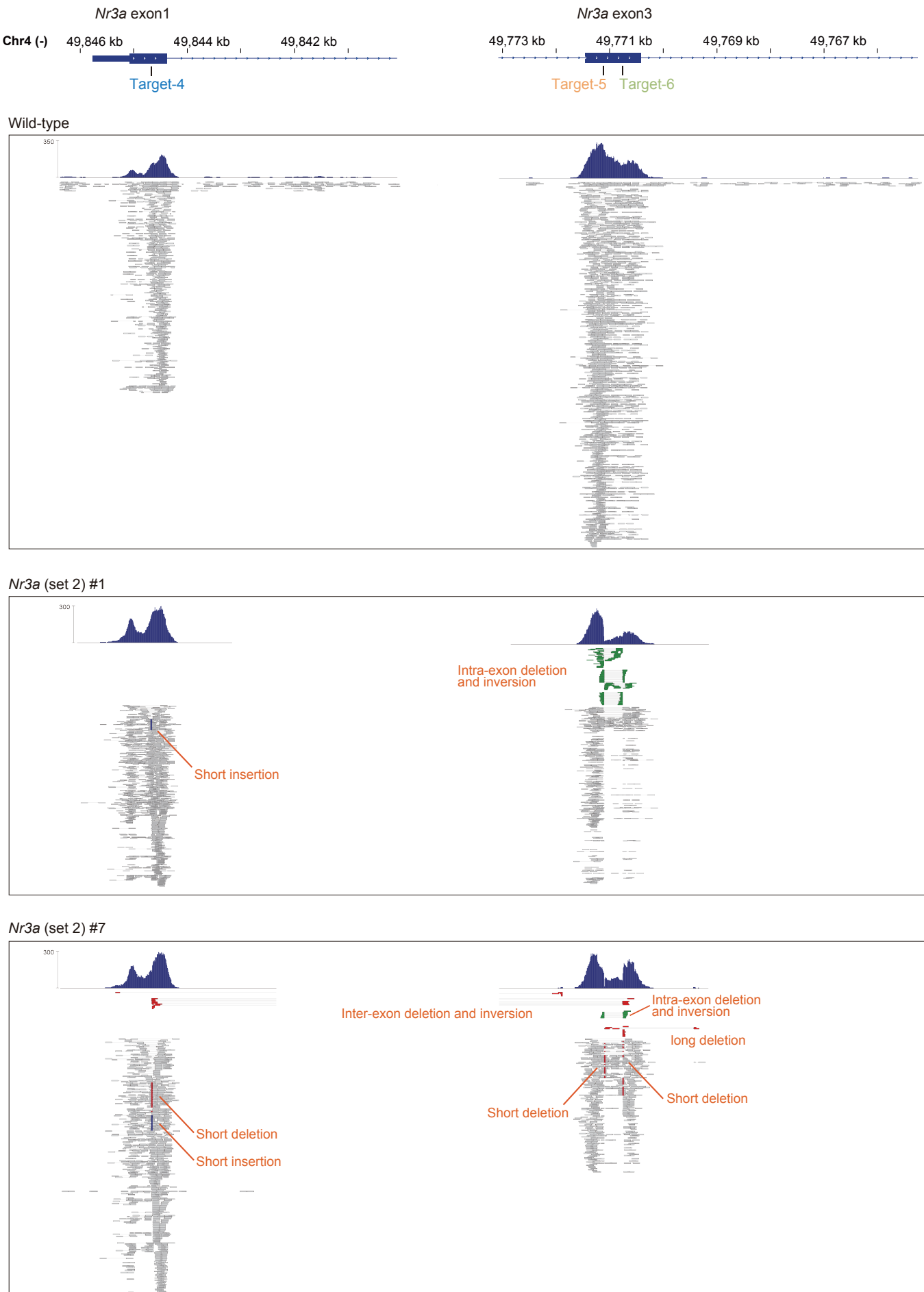


B

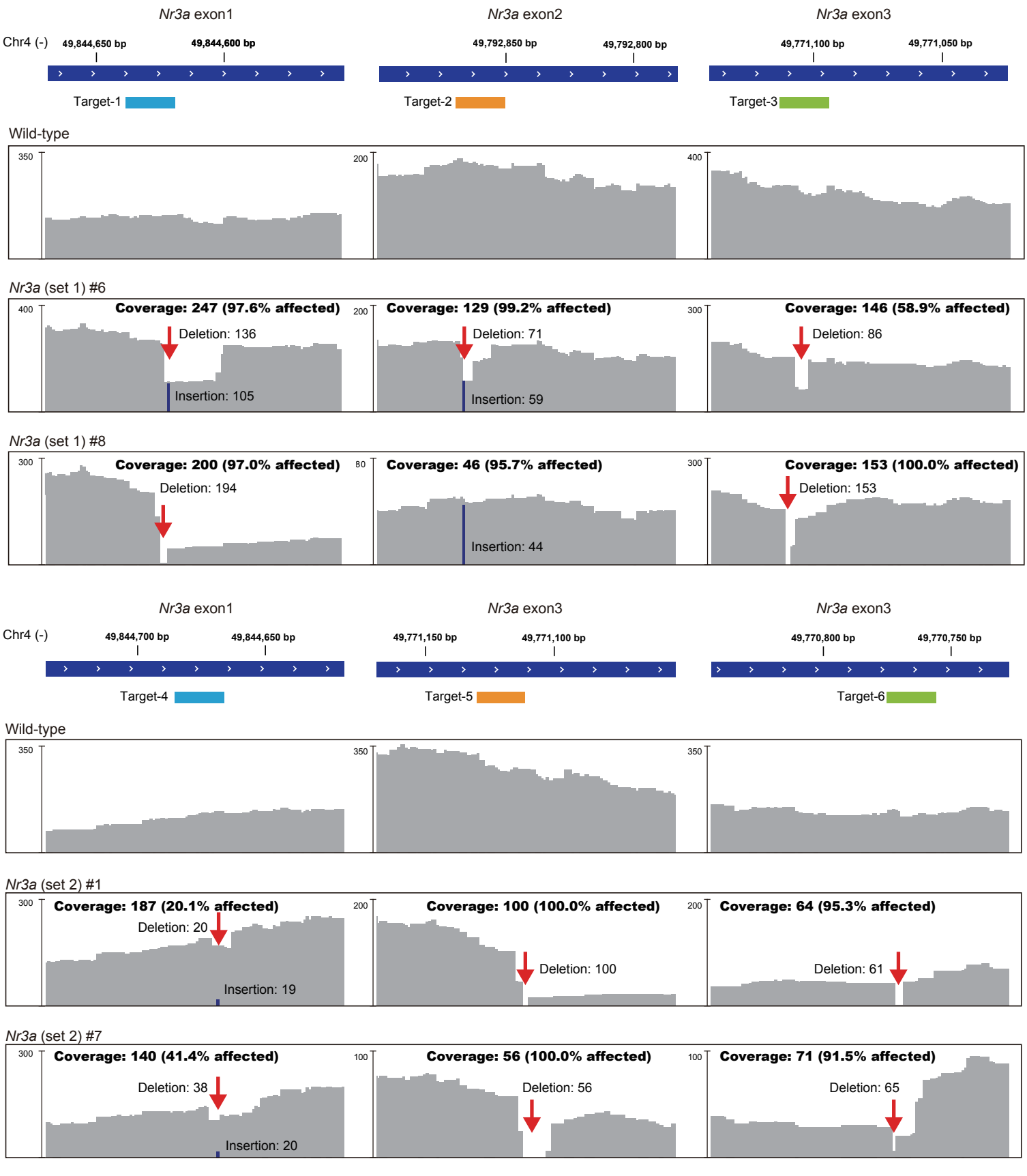


Figure S7 G.A. Sunagawa

**Table S1. Sleep/wake phenotype, Related to Figure 3, 4 and 5.** Every mouse phenotyped in SSS under LD conditions. The values are mean ± SD for wild-type and mean ± SEM for KOs.

| | Strain/gene | # | Daily sleep time (min) | Amplitude | $P_{ws}$ | $P_{sw}$ |
|---|---|---|---|---|---|---|
| Wild-type | C57BL/6N male | 108 | 735.7 ± 50.8 | 0.4462 ± 0.0530 | 0.0379 ± 0.0068 | 0.0363 ± 0.0067 |
| | C57BL/6N female | 72 | 636.4 ± 57.7 | 0.5764 ± 0.0823 | 0.0282 ± 0.0066 | 0.0353 ± 0.0064 |
| | C57BL/6J male | 178 | 699.3 ± 49.6 | 0.4948 ± 0.0610 | 0.0387 ± 0.0064 | 0.0411 ± 0.0076 |
| | C57BL/6J female | 173 | 613.2 ± 50.1 | 0.5716 ± 0.0815 | 0.0300 ± 0.0050 | 0.0406 ± 0.0075 |
| Conventional KO | *Bmal1* | 34 | 719.1 ± 15.0 | 0.3871 ± 0.0132 | 0.0312 ± 0.0014 | 0.0310 ± 0.0012 |
| | *Cry1/Cry2* | 27 | 748.8 ± 11.5 | 0.3586 ± 0.0119 | 0.0331 ± 0.0012 | 0.0307 ± 0.0014 |
| | *Per1/Per2* | 26 | 742.9 ± 14.7 | 0.4308 ± 0.0119 | 0.0456 ± 0.0021 | 0.0431 ± 0.0021 |
| Triple-target CRISPR KO | *Tyr* | 7 | 734.5 ± 17.2 | 0.4249 ± 0.0097 | 0.0368 ± 0.0023 | 0.0350 ± 0.0012 |
| | *Bmal1* | 6 | 758.5 ± 14.6 | 0.3735 ± 0.0189 | 0.0307 ± 0.0022 | 0.0274 ± 0.0015 |
| | *Cry1/Cry2* | 5 | 725.8 ± 14.5 | 0.3489 ± 0.0092 | 0.0388 ± 0.0018 | 0.0381 ± 0.0013 |
| | *Per1/Per2* | 2 | 716.2 ± 2.3 | 0.3699 ± 0.0253 | 0.0364 ± 0.0009 | 0.0368 ± 0.0007 |
| | *Hcrt* | 7 | 720.1 ± 24.1 | 0.3925 ± 0.0278 | 0.0548 ± 0.0022 | 0.0556 ± 0.0048 |
| | *Nr2a* | 8 | 711.9 ± 29.5 | 0.5328 ± 0.0290 | 0.0407 ± 0.0035 | 0.0410 ± 0.0026 |
| | *Nr2c* | 15 | 715.0 ± 11.6 | 0.4557 ± 0.0188 | 0.0343 ± 0.0012 | 0.0348 ± 0.0013 |
| | *Nr2d* | 13 | 755.8 ± 10.6 | 0.4052 ± 0.0131 | 0.0408 ± 0.0011 | 0.0369 ± 0.0010 |
| | *Nr3a* (set 1) | 8 | 639.0 ± 17.5 | 0.5826 ± 0.0342 | 0.0250 ± 0.0015 | 0.0310 ± 0.0009 |
| | *Nr3a* (set 2) | 12 | 627.1 ± 11.2 | 0.5737 ± 0.0169 | 0.0254 ± 0.0009 | 0.0363 ± 0.0006 |
| | *Nr3b* | 11 | 683.7 ± 11.3 | 0.5004 ± 0.0149 | 0.0310 ± 0.0015 | 0.0342 ± 0.0015 |

**Table S2. KO mice production by triple-target CRISPR method, Related to Figure 1, 4 and 5.** *Cas9* mRNA and gRNAs targeting *Tyr* gene and circadian/sleep related genes (*Bmal1*, *Cry1/Cry2*, *Per1/Per2* and *Hcrt*) and NMDA receptor family (*Nr1*, *Nr2a*, *Nr2b*, *Nr2c*, *Nr2d*, *Nr3a*, and *Nr3b*) were injected into fertilized C57BL/6N eggs. Male mice, which surveived at least the age of 6 weeks, were used for SSS analysis. The table shows the number of transferred embryos, number of offsprings and the results of genotyping for all mice used in SSS

| Gene | Transferred embryos | Offspring | | Genotyped male mice | KO confirmed male mice | Non-KO confirmed male mice | Not-determined male mice |
|---|---|---|---|---|---|---|---|
| | | Male | Female | | | | |
| *Tyr* | 150 | 9 | 11 | 7 | 7 | 0 | 0 |
| *Bmal1* | 111 | 6 | 8 | 6 | 6 | 0 | 0 |
| *Cry1/Cry2* | 105 | 6 | 8 | 6 | 5 | 0 | 1 |
| *Per1/Per2* | 169 | 3 | 5 | 3 | 2 | 0 | 1 |
| *Hcrt* | 96 | 11 | 8 | 10 | 7 | 0 | 3 |
| *Nr1* | 205 | 0 | 0 | 0 | 0 | 0 | 0 |
| *Nr2a* | 131 | 8 | 12 | 8 | 8 | 0 | 0 |
| *Nr2b* | 236 | 1 | 0 | 1 | 0 | 1 | 0 |
| *Nr2c* | 143 | 16 | 8 | 15 | 15 | 0 | 0 |
| *Nr2d* | 140 | 13 | 20 | 13 | 13 | 0 | 0 |
| *Nr3a* (set 1) | 135 | 8 | 9 | 8 | 8 | 0 | 0 |
| *Nr3a* (set 2) | 124 | 13 | 7 | 13 | 12 | 0 | 1 |
| *Nr3b* | 205 | 12 | 9 | 12 | 11 | 0 | 1 |
| Total | 1950 | 106 | 105 | 102 | 94 | 1 | 7 |
| | | | | 100.0% | 92.2% | 1.0% | 6.9% |

**Table S5. Exome sequencing statistics for *Tyr* and *Nr3a* KO mice, Related to Figure 2 and 6.** See Methods for the detail of library preparation and sequencing. 'Target bases' are those in bait regions designed for capturing exons.

| Library | Total number of reads | Number of uniquely mapped reads | Uniquely mapped reads (%) | Number of on-bait bases | Proportion of on-bait bases in uniquely mapped reads (%) | Target bases achieving 10X or greater coverage (%) | Sample name in DDBJ |
|---|---|---|---|---|---|---|---|
| Wildtype used in *Tyr* KO analysis | 50,520,378 | 46,336,283 | 91.7 | 3,032,197,583 | 53.7 | 95.0 | tyr-wild-type |
| *Tyr* #1 | 53,635,574 | 49,124,972 | 91.6 | 3,196,839,130 | 53.5 | 95.6 | tyr-01 |
| *Tyr* #2 | 50,975,220 | 47,102,814 | 92.4 | 2,258,383,004 | 39.4 | 91.6 | tyr-02 |
| Wildtype used in *Nr3a* KO analysis | 237,830,634 | 217,074,710 | 91.3 | 13,453,459,028 | 51.0 | 99.0 | nr3a-wild-type |
| *Nr3a* (set 1) #6 | 182,374,702 | 172,485,979 | 94.6 | 14,927,922,341 | 69.9 | 98.9 | nr3a-set1-06 |
| *Nr3a* (set 1) #8 | 194,956,048 | 184,558,103 | 94.7 | 15,510,369,211 | 67.8 | 99.0 | nr3a-set1-08 |
| *Nr3a* (set 2) #1 | 175,181,378 | 167,133,655 | 95.4 | 14,427,136,154 | 69.7 | 98.5 | nr3a-set2-01 |
| *Nr3a* (set 2) #7 | 187,343,854 | 177,780,377 | 94.9 | 15,194,075,796 | 69.0 | 98.8 | nr3a-set2-07 |

Data S1. The Source Code of the SSS Analysis, Written in R Language

The code can be downloaded from **https://goo.gl/teteJM**.